Geophys. J. Int. (2004) **159,** 917–922 doi: 10.1111/j.1365-246X.2004.02476.x

FAST TRACK PAPER

The 2003 Bam (SE Iran) earthquake: precise source parameters from satellite radar interferometry

R. Wang, Y. Xia, H. Grosser, H.-U. Wetzel, H. Kaufmann and J. Zschau

GeoForschungsZentrum Potsdam (GFZ), Telegrafenberg, D-14473 *Potsdam, Germany. E-mail: wang@gfz-potsdam.de*

Accepted 2004 September 20. Received 2004 September 16; in original form 2004 July 26

SUMMARY

Differential radar interferometry provided high-quality near-field deformation data for the 2003 Bam earthquake and therefore strong constraints on its source parameters. The ruptured fault segments could be clearly detected by using a Sobel Edge Filter on the phase-unwrapped deformation field. The estimated total rupture length is about 24 km. More than 80 per cent of the seismic moment was released from its southern segment of about 13 km, where the slip reached a maximum of up to 270 cm resulting in a stress drop of at least 6 MPa. In addition, optical remote sensing data show that the Bam fault is not a single fault but consists of a 4–5 km wide fault system with the known main branch running between the city of Bam and Baravat. The fault ruptured by the Bam earthquake appears to continue the NW branch of this fault system from Bam city southwards. Based on these results, we suggest that the Bam earthquake ruptured a hidden or new fault and that in this process an unusually strong asperity was involved.

Key words: Bam fault, D-InSar, inversion method, slip model.

1 INTRODUCTION

The $M_w = 6.5$ Bam earthquake occurred on 2003 December 26 at 05:56 local time. According to official estimates, more than 26 000 people were killed, about 30 000 injured and up to 75 000 left homeless (http://www.reliefweb.int/).

The city of Bam is located directly in the Bam fault zone and bounds about the known main branch of this fault on the east. The city was built on soft alluvium (erosion deposits and river deposits) where local amplification of the strong ground shaking due to seismic waves are generally expected. The Gowk fault and the Bam fault separate the Zagros collision zone from the relatively rigid Lut block (Berberian *et al.* 2000). The former was considered as the only seismically active fault in this region (Ambraseys & Melville 1982; Walker & Jackson 2002). In the Zagros the convergence rate between the Arabian and Eurasian plates was estimated to be 3.1 cm yr^{-1} (DeMets *et al.* 1990, 1994), but recent GPS studies have shown a lower rate of ∼2.1 cm yr^{-1} (e.g. Sella *et al.* 2002; McClusky *et al.* 2003; Vernant *et al.* 2004). The latter is in good agreement with the recent study of McQuarrie *et al.* (2003) giving a constant rate of ∼2.0 cm yr^{-1} over the last 10 Myr. Moreover, the convergence rate is not only accommodated by the Zagros but also to the north in several areas (Vernant *et al.* 2004). At the SE end of the Zagros, the Gowk and Bam faults are both of the right-lateral strike-slip type accommodating the difference of motion of the Lut block relative to the Central Iranian block (CIB) with a rate of approximately 0.8 cm yr^{-1} (Vernant *et al.* 2004). The differential motion between the Lut and the Central Iranian block are due to the propagation to the north of the transition between the collision of the Zagros (S of CIB) and the Makran subduction (S of Lut). In the Bam region GPS results suggest a motion of only 1.4 cm yr^{-1} (Nilforoushan *et al.* 2003).

The seismically most active fault in the considered region is the Gowk fault (Fig. 1). Five earthquakes of $M_w = 5.4$–7.1 occurred on the Gowk fault since 1981 (Berberian & Yeats 1999; Walker & Jackson 2002), but all are more than 100 km distant from Bam. In comparison, the Bam fault is a comparatively small fault in the region. No strong historical earthquakes have been reported on this fault. Optical remote sensing data (Fig. 1) show that the northern part of the Bam fault is not a single fracture element, but consists of a 4–5 km wide fault system. With data available only from strong distant earthquakes mostly along the Gowk fault, the seismic hazard in the area was rated moderate (i.e. with an expected ground acceleration of up to 2.5 m s^{-2}) to high (3.0 m s^{-2}) for a return period of 75 yr (Tavakoli & Ghafory-Ashtiany 1999). This was an underestimation, because peak ground accelerations of 7.0 –10.0 m s^{-2} were recorded in the epicentral area of the Bam earthquake in both horizontal and vertical directions (Hosseini *et al.* 2004).

From teleseismic data, different agencies determined all a dominant strike-slip mechanism for the Bam earthquake, but their preliminary locations of the epicentre had large errors. The most accurate epicentres given by USGS, Harvard and IIEES differed from each other by 10–18 km. Tatar *et al.* (2004) recorded aftershocks that are

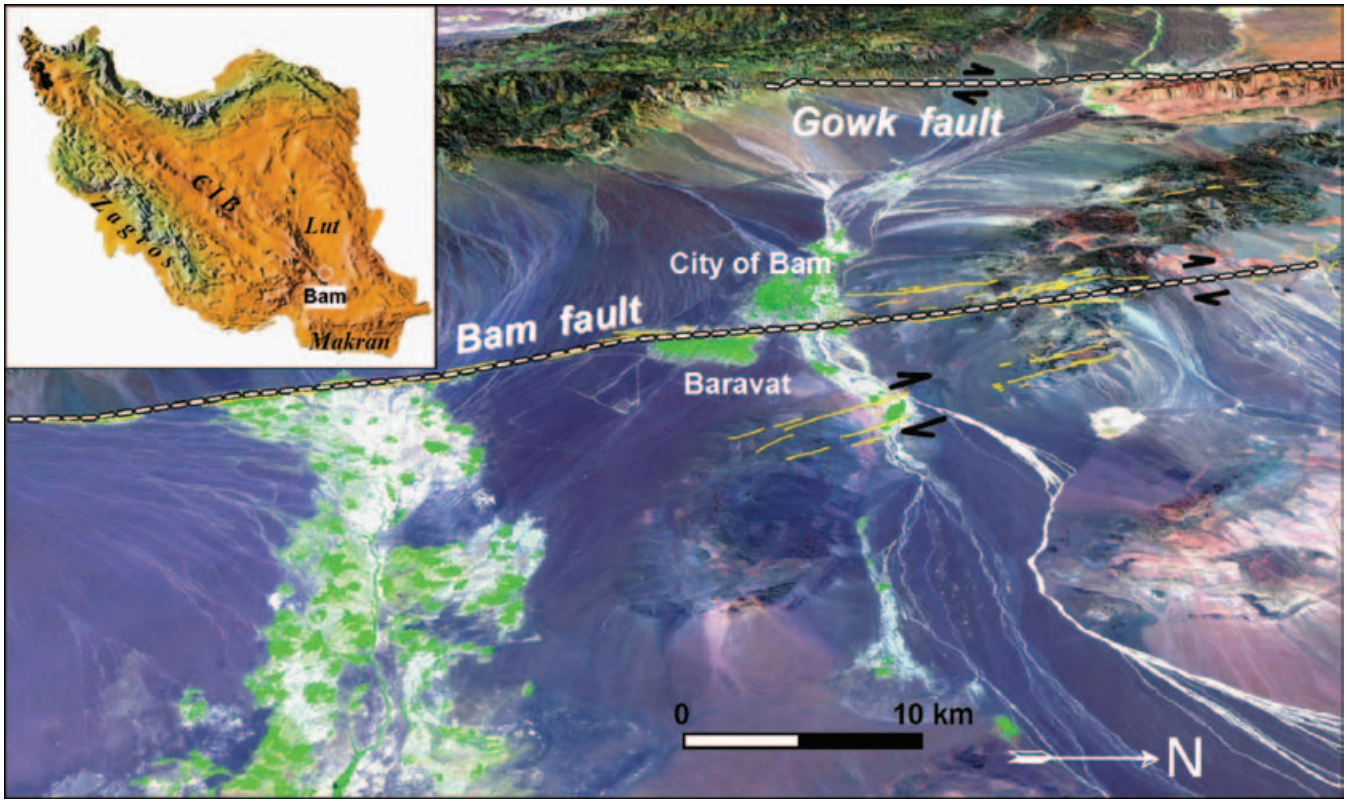

Figure 1. Remote sensing image of Iran (inset) and a perspective view from east to the central part of Bam fault system (ASTER-DEM completed with data of GTOPO30-DEM of EOS Data Center, overlay LANDSAT-TM 159-40, 1987-09-22, bands 7, 4, 1 > R, G, B, processed with Virtual GIS tool of ERDAS-Imagine). Dashed white lines represent the main elements of dextral strike-slip zones of Bam and Gowk (according to Walker & Jackson 2002; modified). Yellow lines show the elements of the Bam fault system from interpretation of the present optical remote sensing data. Directions of the movement of the Gowk fault and interpreted movements of the Bam fault system are marked with black arrows. Note that the scale is valid only for the forefront.

centred in the eastern part of the city of Bam near the known main branch of the Bam fault and have hypocentral depths between 9 and 20 km. From the aftershock distribution, the authors estimated the rupture length of the main shock to be about 18 km.

Differential radar interferometry (D-InSAR) provides high-precision coseismic deformation data which can be used to precisely determine the source parameters (see e.g. Feigl *et al.* 1995). The first successful image of an earthquake's deformation field was obtained by Massonnet *et al.* (1993) for the 1992 Landers earthquake, California. Since then, this technique has been used to map the deformation field of several dozen earthquakes world wide (see e.g. Wright 2002). Recently, Talebian *et al.* (2004) has presented a preliminary source model for the Bam earthquake based on the ENVISAT ASAR descending interferogram. In this paper, we show both descending and ascending interferograms and determine the source model of the Bam earthquake by a joint inversion and by a different inversion method.

2 DIFFERENTIAL SAR INTERFEROMETRY AND DATA PROCESSING

Owing to its arid character, the area of Bam is free of vegetation apart from a few irrigation schemes. Hence, it is perfectly suited for applying the InSAR technique for detection of surface deformation. The European Space Agency provided an ENVISAT ASAR data set for the Bam area including three descending and three ascending pass single look complex images: orbit 6687, 9192, 9693, 8956, 9958 and 10 459, acquired on 2003 June 11, 2003 December 3, 2004 January 7, 2003 November 16, 2004 January 25 and 2004 February 29, respectively. The first two passes were acquired before the event and were used to generate a digital elevation model. The orbit 9693 and 10 459 were acquired after the earthquake and thus contain certainly all information for the co-seismic surface motion due to the strong Bam earthquake in the direction of the satellite's line of sight (LOS). Using the three data pairs (9192/6687, 9192/9693 and 8956/10 459), we generated one interferogram and two differential interferograms.

Though the time interval for our first interferogram is about half a year, the coherence value is still very high and the interferometric fringes are very clear. Phase unwrapping was uncritical. The problem in data processing is the inaccuracy of the ENVISAT orbit parameters. In addition, the passes in the illumination interval, usually about 16 s, are not exactly parallel to each other. As a consequence, some unphysical fringe residues remain in the differential interferograms. In most cases, the residual fringes are significant and have to be removed. Usually, they vary in both directions, from near range to far range and from start acquisition time to stop time. The estimation of the ratio between the residual fringes and the baseline correction therefore becomes difficult. To solve this problem, the interferometric phase of the selected ellipsoid reference surface was not directly computed from the parallel baseline, but based on the estimation of the interferometric fringe frequency pattern of the reference surface (Xia *et al.* 2003).

The differential interferograms show the coseismic displacements of the 2003 Bam earthquake mapped in the LOS direction in

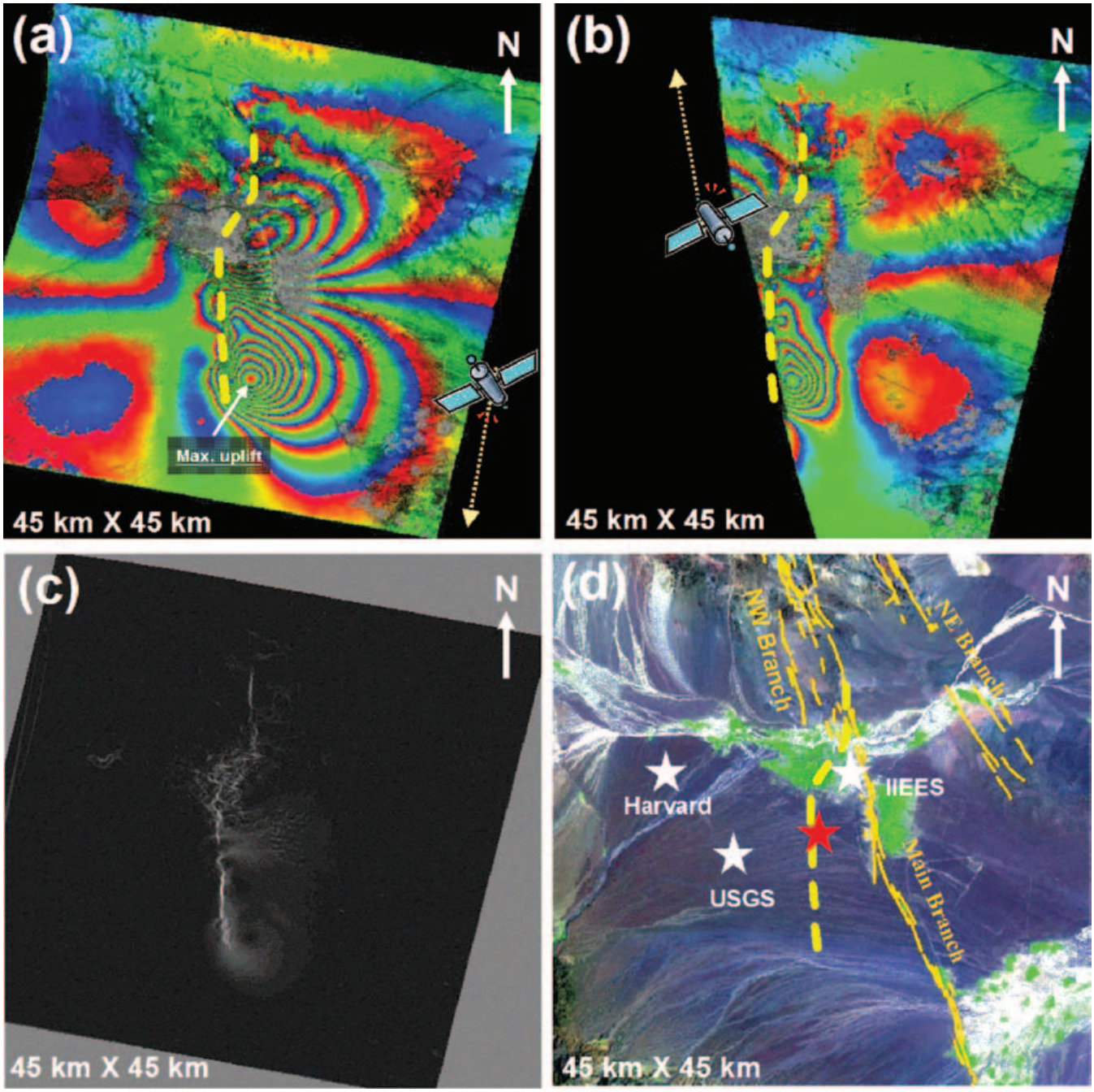

Figure 2. Differential ENVISAT ASAR interferograms (geocoded) (a) from the data pair of descending orbit 9192 and 9693 and (b) from the data pair of ascending orbit 10 459 and 8956. The geo-coded area are limited by the ASTER's DEM. Each fringe step represents a LOS displacement of 2.8 cm. The software GFZ-InSAR developed by the GeoForschungsZentrum Potsdam (GFZ) was used for the data processing. (c) shows the Sobel Edge filtered descending LOS displacements for detecting the rupture trace, and (d) the derived fault (dotted yellow line) ruptured by the 2003 Bam earthquake drawn on the optical image. Red star marks the location at (29.052°N, 58.365°E), where the slip reached a maximum of up to 270 cm in the depth of 2–4 km. White stars show a few teleseismic locations of the epicentre (http://www.emsc-csem.org, 2003).

descending and ascending passes (Figs 2a and b), respectively. Each colour period represents a LOS displacement of 2.8 cm. Both differential interferograms were geocoded with a digital elevation model (DEM) derived from ASTER optical data. In the case of descending orbit, the maximum uplift along the LOS reaches about 30 cm and is located at (28.981°N, 58.381°E) ± 100 m. The maximum subsidence cannot be located such accurately. It is about 18 cm at about 12 km north from the maximum uplift.

3 INVERSION FOR THE SOURCE PARAMETERS

In order to detect the ruptured fault on the surface, a Sobel Edge Filter was used on the phase-unwrapped deformation field. This is based on the fact that the horizontal gradient of the deformation should take its maximum near and along the ruptured fault. From the filtered data, we could clearly identify the position and

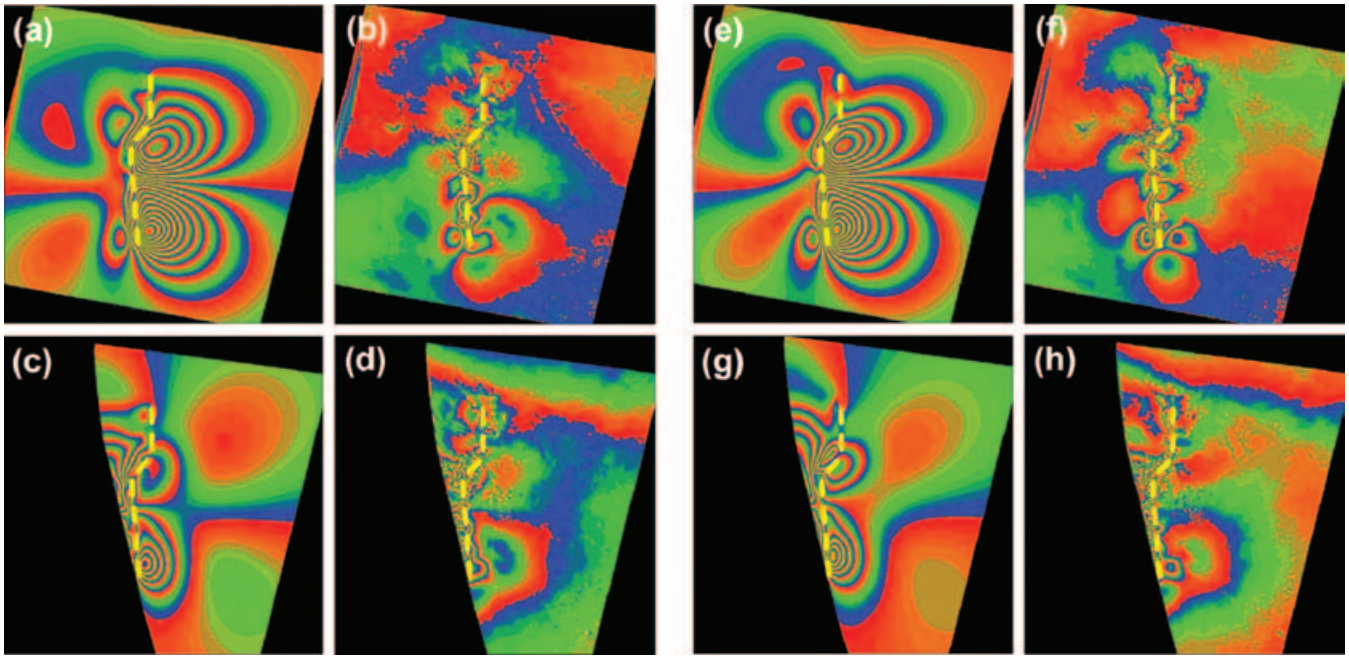

Figure 3. Modelling results for the surface deformation of the 2003 Bam earthquake. Left: (a) and (b) show the predicted and residual descending ENVISAT ASAR interferograms, respectively, using the slip model obtained from the successive approximation method (Fig. 4a). (c) and (d) are the same as (a) and (b), but for the ascending data. Right: (e)–(h) are as same as (a)–(d), but using the slip model obtained from the least-squares method (Fig. 4b). The dotted yellow line marks the fault ruptured by the earthquake.

orientation of the ruptured fault (Fig. 2c). Approximately, it consists of three straight segments. The southern segment is about 13 km and runs from (28.971°N, 58.357°E) to (29.088°N, 58.351°E), and the northern one is about 6 km from (29.126°N, 58.382°E) to (29.178°N, 58.382°E). The middle one disappeared below the city area of Bam, where a lack of coherence prevents its tracking. For simplicity, we suppose that the fault in this area connects the southern and northern segments. The connecting line is about 5 km, so then the total length of the ruptured fault is estimated to be 24–26 km. Drawing them on the optical image (Fig. 2d), we see that the main southern segment is located at 4–5 km west to the known main branch of the Bam fault, whereas the northern segment coincides with it.

The earthquake was therefore simulated by three rectangular fault planes with length and strike of (14 km, 357°), (5 km, 35°) and (7 km, 0°), respectively. From a number of forward modelling runs, we found that the southern and middle fault planes dip 75–80° to the east, while the northern one dips 55° to the west. The maximum width of the ruptured area reaches about 12 km. In the next step, we fixed this fault geometry and determined the inhomogeneous slip distribution by a joint inversion from both descending and ascending ENVISAT ASAR interferograms (Figs 2a and b). To increase the computation efficiency, the InSAR data were filtered to a spatial resolution of 0.5 × 0.5 km^2. A comparable spatial resolution was used to discretize the rupture area, resulting in about 1200 point sources to be determined from about 250 000 and 150 000 observed displacements in the descending and ascending LOS directions, respectively.

A direct inversion for such a large number of discrete slip vectors is not only time-consuming but may also involve stability problems. For example, the derived slip distribution, which gives the best-fit to the data, may exhibit an unrealistic oscillatory character. To solve this problem, some artificial constraints such as smoothing the slip field and/or restricting the slip to a given direction are usually required (e.g. Pedersen *et al.* 2003). Here we propose a different inversion algorithm, in which the slip distribution is developed to a series of bi-orthogonal functions,

$$\mathbf{S}(x, y) \approx \sum_{n=1}^{N} \sum_{m=1}^{M} \mathbf{S}_n^m f_n(x) f_m(y), \tag{1}$$

where $x \in (0, 1)$ and $y \in (0, 1)$ are the normalized coordinates along the fault length and width, respectively, $\mathbf{S}(x, y)$ is the slip vector at the position (x, y), $f_n(x)f_m(y)$ are the bi-orthogonal functions (in the present case we used $f_n(x) f_m(y) = \sin\, n\pi x \, \sin m\pi y$) of degree n and m in the strike and dip directions, respectively, and $\mathbf{S}_n^m$ are the corresponding slip vector coefficients to be determined.

For shallow events, such as the Bam earthquake, we may suppose that any two orthogonal slip terms will produce two incoherent surface deformations. Under this condition, the coefficients $\mathbf{S}_n^m$ in eq. (1) can be determined successively from term to term, so that the computation efficiency is considerably increased in comparison with the direct inversion method. In the present case, such condition is more or less satisfied for the low-degree (long wave length) slip terms. Therefore, we start with the lowest degree $(n, m) = (1, 1)$ and determine the term $\mathbf{S}_1^1$ by e.g. the least-squares fitting to the observed LOS displacements. The remaining residuals should be caused by terms of higher degrees. In the next step, we then process the degree (1,2) or (2,1) and determine the corresponding slip term $\mathbf{S}_1^2$ or $\mathbf{S}_2^1$ by fitting the residuals remaining after the first step, and so on up to the cut-off degree (N, M). This new inversion approach may be called the successive approximation (SA) method. The advantage of this method is that one can always obtain a stable slip distribution with a resolution as high as resolvable from the data. Additional constraints such as smoothing are not needed.

For comparison, we also solved the complete set of the slip coefficients simultaneously by the least-squares (LS) fitting method with the smoothing condition. A similar approach has been used by Pollitz *et al.* (1998). The modelling results from the two different

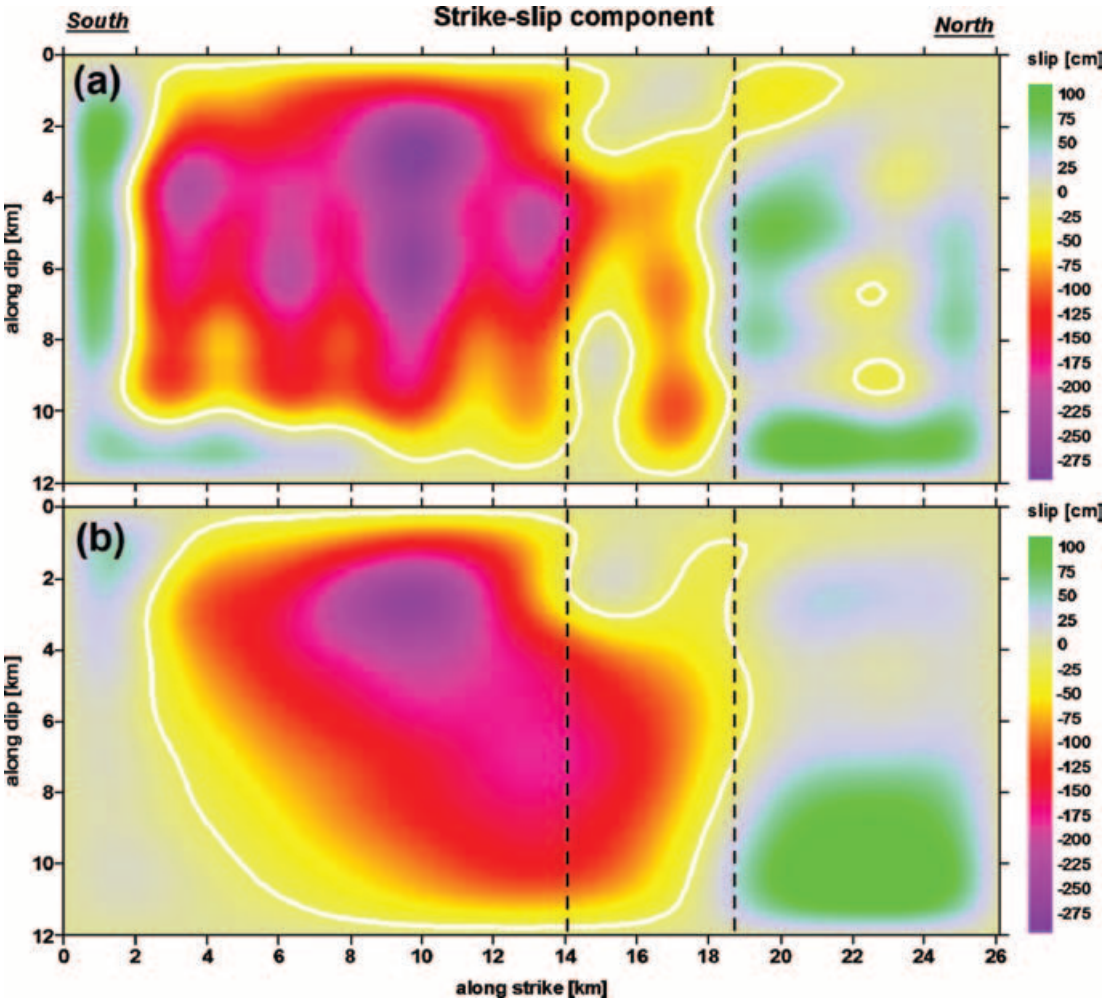

Figure 4. The best-fitting slip models (strike-slip component) inversed from the two differential ENVISAT ASAR interferograms shown in Fig. 2 by using (a) the successive approximation method and (b) the least-squares fitting method with the smoothing condition. The cut-off degrees of the slip distribution [see eq. (1)] are $N = 16$ and $M = 8$ for the strike and dip directions, respectively. The thick white line is the −25 cm contour (negative = right-lateral), marking about the rupture area. The dip-slip component for both models is about one order smaller than the strike-slip component and is not shown here. Dotted lines mark the connecting positions of the different fault segments.

methods are compared in Fig. 3 and the corresponding best-fitting slip models in Fig. 4.

In general, the LOS displacements observed in both descending and ascending LOS directions can be well simulated by the two different fitting methods. The maximum residuals are all smaller than 10 cm and only appear near the fault because of local irregularities of the rupture. Measuring by the root-mean-square residual, however, the fitting quality of the successive approximation (1.0 cm for the descending data and 1.3 cm for the ascending data) are significantly better than that of the least-squares method (2.7 and 2.1 cm).

Both slip models (Fig. 4) show a nearly pure strike-slip mechanism for the earthquake. More than 80 per cent of the seismic moment was released from the southern fault segment. The slip direction is right-lateral as expected for the Bam fault. The magnitude of the slip on the northern segment is significantly smaller and seems to be not clearly resolvable by both inversion methods. We suggest that this part of surface rupture may be caused by shallow local effects due to the strong ground shaking. In particular, the same moment magnitude of $M_w = 6.5$ has been derived from the two slip models (Fig. 4). Other important parameters such as the spatial extension of the ruptured area ($\sim 16 \times 12$ km^2), the maximum slip ($\sim$270 cm) as well as its location ($\sim$10 km from the southern end and at $\sim$3 km depth) are in agreement, too. In comparison, it appears that the slip distribution was better resolved by the SA method than by the LS method.

4 DISCUSSION AND CONCLUSIONS

Differential ENVISAT ASAR interferometry has provided high-quality deformation data for the $M_w = 6.5$ Bam (SE Iran) earthquake of 2003 December 26. Using the two data sets obtained from both descending and ascending orbit pairs, we could precisely determine the source parameters of the strong 2003 Bam earthquake. The fault-plane solution indicates that it was a right-lateral strike-slip earthquake as expected for the Bam fault. The derived rupture area strikes from south to north. The total length of the ruptured fault is about 24 km and consists of three segments. More than 80 per cent of the seismic moment was released from the southern fault segment of 13–14 km, where the slip reached a maximum of up to 270 cm. According to Wells & Coppersmith (1994), this slip value is unusually large for a $M_w = 6.5$ earthquake. It results consequently

in an unusually high stress drop of at least 6 MPa on this fault segment, implying that a strong asperity was involved in the rupture process.

The nearly NS orientation of the ruptured fault corresponds about to that of the known main branch of the Bam fault between the city of Bam and Baravat. The present results suggest, however, that the earthquake ruptured a hidden or new fault which dips by about 80° to east and is located 4–5 km west from this main branch. Drawing the ruptured fault on the optical remote sensing image (Fig. 2d), we see that the earthquake appears to have continued the NW branch of the Bam fault system from Bam city southwards.

In our source model, we have considered three fault segments which were detected by using a Sobel Edge Filter on the phase-unwrapped deformation field. In comparison, Talebian *et al.* (2004) constructed their source model by adopting the mechanism from teleseismic observations. It consists of the main strike-slip fault (strike 357°, dip 88°, and rake −166°), and an additional pure thrust fault (strike 180°, dip 30°, and rake 90°). The strike-slip fault corresponds about to the southern fault segment of our source model shown in Fig. 2(c). The thrust fault is located at 10 km east and nearly parallel to the strike-slip fault. Though it is difficult to imagine how these two contradictory faults interact with each other, the modelling results of these authors give the impression that the combination of the two faults is necessary for explaining the descending interferogram (see their Auxiliary Fig. 4). From the present study, we could verify the main strike-slip fault, but found no evidence for the second, thrust fault at the given location. Both descending and ascending interferograms can be satisfactorily predicted when the fault geometry is used which is directly derived from the InSAR data.

ACKNOWLEDGMENTS

We thank the European Space Agency for providing the ENVISAT ASAR data. S. M. Richwalski read the manuscript and gave constructive suggestions for improvement. M. Motagh provided useful information about the Bam area. Comments and suggestions from P. Vernant and M. Wyss were very helpful for improving the paper.

REFERENCES

Ambraseys, N.N. & Melville, C.P., 1982. *A history of Persian earthquake,* the University Press, Cambridge.

Berberian, M. & Yeats, R.S., 1999. Patterns of historical earthquake rupture in the Iranian plateau, *Bull. seism. Soc. Am.,* **89,** 120–139.

Berberian, M., Jackson, J.A., Qorashi, M., Talebian, M., Khatib, M. & Priestley, K., 2000. The 1994 Sefidabeh earthquake in eastern Iran: blind thrusting and bedding-plane slip on a growing anticline, and active tectonics of the Sistan suture zone, *Geophys. J. Int.,* **142,** 283–299.

DeMets, C., Gordon, R.G., Argus, D.F., & Stein, S., 1990. Current plate motions, *Geophys. J. Int.,* **101,** 425–478.

DeMets, C., Gordon, R.G., Argus, D.F., & Stein, S., 1994. Effects of recent revisions to the geomagnetic reversal time scale on estimates of current plate motions, *Geophys. Res. Lett.,* **21,** 2191–2194.

Feigl, K.L., Sergent, A. & Jacq, D., 1995. Estimation of an earthquake focal mechanism from a satellite radar interferogram: application to the December 4, 1992 Landers aftershock, *Geophys. Res. Lett.,* **22,** 1037–1048.

Hosseini, K.A., Mahdavifar, M.R., Bahshayesh, M.K. & Rakhshandeh, M., 2004. Engineering geology and geotechnical aspects of Bam earthquake (preliminary report), http://www.emsc-csem.org/.

Massonnet, D., Rossi, M., Carmona, C., Adragna, F., Peltzer, G., Feigl, K. & Rabaute, T., 1993. The displacement field of the Landers earthquake mapped by radar interferometry, *Nature,* **364,** 138–142.

McClusky, S., Reilinger, R., Mahmoud, S., Ben Sari, D. & Tealeb, A., 2003. GPS constraints on Africa (Nubia) and Arabia plate motions, *Geophys. J. Int.,* **1,** 126–138.

McQuarrie, N., Stock, J.M., Verdel, C. & Wernicke, B.P., 2003. Cenozoic evolution of Neotethys and implications for the causes of plate motions, *Geophys. Res. Lett.,* **30,** doi:10.1029/2003GL017992.

Nilforoushan, F. *et al.*, 2003. GPS network monitoring the Arabia-Eurasia collision deformation in Iran, *Journal of Geodesy,* **77,** 411–422.

Pedersen, R., Jónsson, S., Árnadóttir, T., Sigmundsson, F. & Feigl, K.L., 2003. Fault slip distribution of two June 2000 Mw 6.5 earthquakes in South Iceland estimated from joint inversion of InSAR and GPS measurements, *Earth planet. Sci. Lett.,* **213,** 487–502.

Pollitz, F.F., Bürgmann, R. & Segall, P., 1998. Joint estimation of afterslip rate and postseismic relaxation following the 1989 Loma Prieta earthquake, *J. geophys. Res.,* **103,** 26 975–26 992.

Sella, G.F., Dixon, T.H. & Mao, A., 2002. REVEL: A model for recent plate velocities from space geodesy, *J. geophys. Res.,* **107,** doi:10.1029/2000JB000033.

Talebian, M. *et al.*, 2004. The 2003 Bam (Iran) earthquake: rupture of a blind strike-slip fault, *Geophys. Res. Lett.,* **31,** doi:10.1029/2004GL020058.

Tatar, M., Javan, D., Farabhod, A., Paul, A. & Hatzfeld, D., 2004. Aftershock seismicity of the Bam earthquake, European Geosciences Union —1st General Assembly (Abstract EGU04-A-07893), Nice, France, 25–30April.

Tavakoli, B. & Ghafory-Ashtiany, M., 1999. Seismic hazard assessment of Iran, *Annali di Geofisica,* **42,** 1013–1021.

Vernant, P. et al, 2004. Contemporary crustal deformation and plate kinematics in Middle East constrained by GPS measurements in Iran and Northern Oman, *Geophys. J. Int.,* **157,** 381–398.

Walker, R. & Jackson, J., 2002. Offset and evolution of the Gowk fault, S.E. Iran: a major intra-continental strike-slip system, *Journal of Structural Geology,* **24,** 1677–1698.

Wells, D.L. & Coppersmith, K.J., 1994. New empirical relationships among magnitude, rupture width, rupture area, and surface displacement, *Bull. seism. Soc. Am.,* **84,** 974–1002.

Wright, T.J., 2002. Remote monitoring of the earthquake cycle using satellite radar interferometry, *Phil. Trans. R. Soc. Lond.,* **360,** 2873–2888.

Xia, Y., Michel, G.W., Reigber, Ch., Klotz, J. & Kaufmann, H., 2003. Seismic unloading and loading in northern central Chile as observed by differential Synthetic Aperture Radar Interferometry (D-InSAR) and GPS, *Int. J. Remote Sensing,* **24,** 4374–4391.